A Flexible Bandpass Filter Design Procedure Applied to Midlatitude Intraseasonal Variability

FRANCISCO J. DOBLAS-REYES AND MICHEL DÉQUÉ

Centre National de Recherches Météorologiques, Météo-France, Toulouse, France

(Manuscript received 7 July 1997, in final form 30 December 1997)

ABSTRACT

A general digital bandpass filtering procedure is presented whose advantages over other simple filtering methods are 1) versatility in its design, because only a set of three parameters is needed to calculate the filter weights via a simple analytic expression, 2) good performance at the transition band depending on the number of weights considered, and 3) the reduction of the Gibbs oscillations in the pass band of a given raw filter by convolving it with a convergence window. In order to illustrate the method, the filter has been first used to assess the ability of the Météo-France general circulation model ARPEGE to simulate the midtropospheric low-frequency intraseasonal variability in the Northern Hemisphere. The filter examined here allows one to assess the model drawbacks in different frequency bands. As a second example, the synoptic-scale baroclinic fluctuations in midlatitudes have also been studied. It is shown that the horizontal and vertical structure of these fluctuations does not depend very much on the frequency band up to a period of 10 days, but shows an increase in zonal wavelength as lower-frequency fluctuations are considered.

1. Introduction

There is a need in climate studies to have efficient procedures for isolating the target variability from the total spectrum. Digital filtering is one such procedure that is widely applied, for example, to initialization of numerical weather prediction models in order to reduce gravity wave components to a realistic level (Huang and Lynch 1993). Such applications have shown that the simplicity of calculating the filter weights and an adequate filter response are two desirable properties. Duchon (1979) offered a thorough picture of what could be done with Lanczos-type digital filtering, and his expressions have been used in many later studies, such as those of Kousky and Kayano (1994) and Lanzante (1996). However, many predefined filters (i.e., those using weights tabulated in previously published works) have been applied, such as the low-pass and bandpass filters proposed by Blackmon (1976) or Blackmon and Lau (1980). The use of these filters can produce confusion when the results are analyzed. For example, Déqué and Piedelievre (1995) obtained insight into the ARPEGE (a French acronym meaning small- and large-scale research project) general circulation model (GCM) variability by filtering with one of the latter filters. They found that the model undersimulated the midlatitude low-pass filtered 500-hPa geopotential height standard deviation. There was uncertainty about which timescales were causing this underestimation: either interannual (IA) or intraseasonal (IS) scales. This is because anomalies computed with the Blackmon low-pass filter always retain a portion of IA variability, so that the use of an easy-to-define bandpass filter would have been more appropriate in this case in order to isolate the IS fluctuations.

Digital bandpass filtering is a widely used method in studies of weather and climate variability. For a specific study, one is tempted to use a predefined filter because they have been previously tested, although some limitations can often be found due to inadequacies in the frequency response. However, there is often a need for a family of filters adapted to the timescales one may be interested in. For such problems a new set of filter weights has to be computed and this task is rendered much simpler if simple analytic expressions exist for the filter weights, as was presented in Duchon (1979). However, simple analytic filters are often far from being excellent. For example, the poor man's filter described in Hoskins et al. (1989) is too specific and has a poor frequency response. Thus, the generalization of a simple efficient bandpass filter design defined by a small set of parameters and suitable for being applied to any particular situation desired may be very useful. The purpose of this paper is to present such a procedure for obtaining filter weights computed easily from simple analytic expressions and that can be adapted for any specific problem. In section 2, the method is introduced and in section 3 it is illustrated with two examples.

Corresponding author address: Dr. Francisco Doblas-Reyes, CNRM, Météo-France, 42, ave. G. Coriolis, 31057 Toulouse, France. E-mail: reyes@cnrm.meteo.fr

2. Filtering procedures

a. The transfer function

A linear symmetric digital filtering of the discrete time series z_k, $k = 1, \ldots, N$ may be expressed as the convolution

$$u_k = \sum_{j=-S}^{S} w_j z_{k-j}, \tag{1}$$

where w_j are the filter weights (satisfying $w_j = w_{-j}$) and S is the filter span. The total number of weights is $2S + 1$, so that the filtered time series exists for $k = S + 1, \ldots, N - S$.

Fourier spectral representation is of particular value when digital filtering is used because the functions $\exp(ik\theta)$ are eigenfunctions of the filtering operation (Hamming 1977). The corresponding eigenvalue $T(\theta)$ is the transfer function (or frequency response function) of the filter

$$T(\theta) = \sum_{j=-S}^{S} w_j e^{-ij\theta}. \tag{2}$$

It describes in frequency space the way in which a sinusoid with frequency θ is transferred from the input to the output by the linear filter. Its squared magnitude is called the power transfer function and, if P_z is an estimate of the spectrum of z_k, the following relation holds:

$$P_u(\theta) = |T(\theta)|^2 P_z(\theta), \tag{3}$$

showing that $T(\theta)$ modulates the spectrum of u_k. As only symmetric filtering and real-valued data are considered here, there is no phase shift of the signal after filtering (note that $T(\theta)$ is real valued).

It should be noted that many atmospheric fluctuations present nonstationary evolution, as, for instance, the seasonal evolution of blocking activity or the midwinter suppression of the Pacific storm track. Stationarity is useful if filter simplicity is sought, and it can be achieved by prior removal of an estimate of the mean annual cycle (prewhitening). In this context, the power transfer function can still be a powerful tool for evaluating filters.

b. Low-pass filtering

Low-pass filtering can be used to elegantly define bandpass filters and so a brief discussion of this type of filtering is given. A low-pass filter suppresses all components with frequency higher than a certain value. Its transfer function should be close to 1 for frequencies in the interval associated with the low-frequency component (the pass band) and close to 0 elsewhere (stop band). An ideal low-pass filter with frequency cutoff θ_c (the highest frequency with nonzero power transfer function) is given by

$$T(\theta) = \begin{cases} 1 & 0 \le |\theta| \le \theta_c \\ 0 & \theta_c < |\theta| \le \pi. \end{cases} \tag{4}$$

Filter weights are obtained as the Fourier transform of $T(\theta)$,

$$w_j = \frac{1}{2\pi} \int_{-\theta_c}^{\theta_c} e^{ij\theta}\, d\theta \qquad -\infty < j < +\infty, \tag{5}$$

but in practice this series must be truncated to a finite series. If we consider $2S + 1$ terms,

$$w_j = \begin{cases} \dfrac{\theta_c}{\pi} & j = 0 \\ \dfrac{\sin(j\theta_c)}{j\pi} & 0 < |j| \le S \\ 0 & |j| > S. \end{cases} \tag{6}$$

Any finite length filter will depart from an ideal filter in that there will be few, if any, points at which the transfer function will have exactly the values 0 or 1 and there will be a finite ''transition band'' in which the transfer function drops from values near 1 at the pass frequency θ_p to nearly 0 at the stop frequency θ_s. The transition band width may be approximated by $\delta = \theta_s - \theta_p$. An additional problem that may occur is the appearance of undesired oscillations in the transfer function, an effect known as the ''Gibbs phenomenon,'' which is due to overshooting in the filter response (transfer function greater than 1 in the pass band and less than 0 in the stop band) (Christoph et al. 1995). In general terms, frequency response can be expressed as an infinite Fourier series. However, as shown above, only a finite number of terms is used. Such a truncation introduces discontinuities and spurious oscillations appear in the transfer function, which are known as Gibbs oscillations. The truncation in Eq. (6) produces Gibbs oscillations in the transfer function [see Bloomfield (1976, 132) for examples of the phenomenon]. It is desirable to reduce this problem as much as possible. To control Gibbs oscillations and achieve a high accuracy of approximation to the ideal filter, the low-pass filter frequency response can be smoothed. Some windows may be combined with the truncated least squares low-pass filter. These windows (denoted henceforth as d_j) are known as convergence windows and are applied by multiplying w_j pointwise by the window value d_j to obtain the smoothed filter weights $\tilde{w}_j = w_j d_j$, representing a convolution in the frequency domain. This achieves the required smoothing of the low-pass transfer function of w_j, eliminating a great part of the Gibbs oscillations.

c. Convergence windows

In this paper, two types of convergence windows have been considered. One is defined by Bloomfield (1976) and has been used, among others, by Enting (1987) and

Valero et al. (1996). It is equivalent to a Lanczos window (Duchon 1979) and is defined as

$$d_j^B = \frac{\sin(\theta_j)}{\theta_j}, \tag{7}$$

where $\theta_j = 2\pi j/(2S + 1)$. It is important to note the parsimony of this window, which depends solely on the span S. As the wavelength of the ripples in the transfer function of w_j to be smoothed is $\delta = 4\pi/(2S + 1)$ (Bloomfield 1976), the window is chosen as a function of this feature. The parameter δ coincides with the transition band width. This shows that for obtaining a faster transition from the pass band to the stop band, that is, a sharp cutoff, we have to increase S. Finally, the effect of this window is to produce a modified transfer function that decays almost linearly from the value 1 at $\theta_c - \delta/2$ to 0 at $\theta_c + \delta/2$.

Another useful convergence window is the Dolph–Chebyshev (hereafter referred to as Dolph) window (Dolph 1946; Lynch 1997; Lynch et al. 1997). Coefficients are given by

$$d_j^D = \frac{1}{2S+1}\left[1 + 2r \sum_{m=1}^{S} T_{2S}\left(x_0 \cos\frac{\theta_m}{2}\right)\cos(m\theta_m)\right], \tag{8}$$

where $T_{2S}(x)$ is the $2S$th order Chebyshev polynomial, S is the filter span, $r = 1/T_{2S}(x_0)$ and represents the maximum amplitude of the window transfer function in the stop band, and x_0 is a parameter greater than 1 defined by

$$x_0 \cos\frac{\theta_s'}{2} = 1, \tag{9}$$

where θ_s' is the window stop band edge. One remarkable aspect of this window is that it has an analytic expression for the finite Fourier transform (which the Bloomfield window does not):

$$T(\theta) = \frac{T_{2S}\left(x_0 \cos\frac{\theta}{2}\right)}{T_{2S}(x_0)}. \tag{10}$$

The price to be paid for this useful property is that the expressions for the coefficients d_j^D are more difficult to compute than are those for d_j^B. The filter coefficients d_j^D are determined by three parameters: S, r, and θ_s'. In order to use it as a convergence window we have stated the window stop band edge θ_s' and the filter span S (Lynch 1997), so that r is given by

$$\frac{1}{r} = \cosh(2S \cosh^{-1} x_0). \tag{11}$$

This choice produces minimum ripples for a given transition band width and filter span. The choice used here sets $\theta_s' = \delta$ and provides an optimal convergence window.

d. Bandpass filtering

A bandpass filter is different from a low-pass filter in that both low-frequency and high-frequency components are removed. The previous low-pass filters offer the possibility of analytically designing a simple bandpass filter, which can permit the user to flexibly define the filter features depending on the study goals. In order to construct the bandpass filter, we introduce two different low-pass filter versions of z_k with cutoff frequencies θ_c^l and θ_c^u, where $\theta_c^l < \theta_c^u$. Let us suppose that both filters are of the same length (i.e., they have the same span). If the two output time series are then subtracted, the result corresponds to a bandpass filtering process. The bandpass filtered time series x_k is given by

$$x_k = \sum_{j=-S}^{S} (w_j^u - w_j^l) z_{k-j} = \sum_{j=-S}^{S} b_j z_{k-j}, \tag{12}$$

where w_j^u, w_j^l are the weights for the upper and lower cutoff low-pass filter weights, respectively. The filter transfer function is given by

$$T(\theta) = \sum_{j=-S}^{S} b_j e^{-ij\theta} = T_u(\theta) - T_l(\theta). \tag{13}$$

This equation means that b_j are the weights of a filter that removes the lowest-frequency components [because both $T_u(\theta)$ and $T_l(\theta)$ are close to 1 for the lowest frequencies], and the frequency components higher than θ_c^u.

When the previous low-pass filters are used for building the bandpass filter, the corresponding weights are given by

$$b_j = \begin{cases} d_0 \dfrac{B\theta_c^u - A\theta_c^l}{AB\pi} & j = 0 \\ \dfrac{d_j}{AB\pi j}(B \sin j\theta_c^u - A \sin j\theta_c^l) & 0 < |j| \le S, \end{cases} \tag{14}$$

where A and B are normalizing factors,

$$A = \frac{d_0\theta_c^u}{\pi} + 2\sum_{j=1}^{S} \frac{d_j \sin j\theta_c^u}{\pi j}$$

$$B = \frac{d_0\theta_c^l}{\pi} + 2\sum_{j=1}^{S} \frac{d_j \sin j\theta_c^l}{\pi j}, \tag{15}$$

needed to give the correct combination of the two low-pass filters. The bandpass filter is then defined by *only* three parameters (independently of the convergence window): the upper and lower cutoff frequencies θ_c^u, θ_c^l, and the filter length S. The same result would have been obtained by convolving the bandpass obtained from the least squares low-pass filter with the convergence windows in order to improve the transfer function.

To illustrate the method, the transfer function was calculated for bandpass filters using both convergence windows with $\theta_c^u = 2\pi/10$ and $\theta_c^l = 2\pi/90$, that is, a

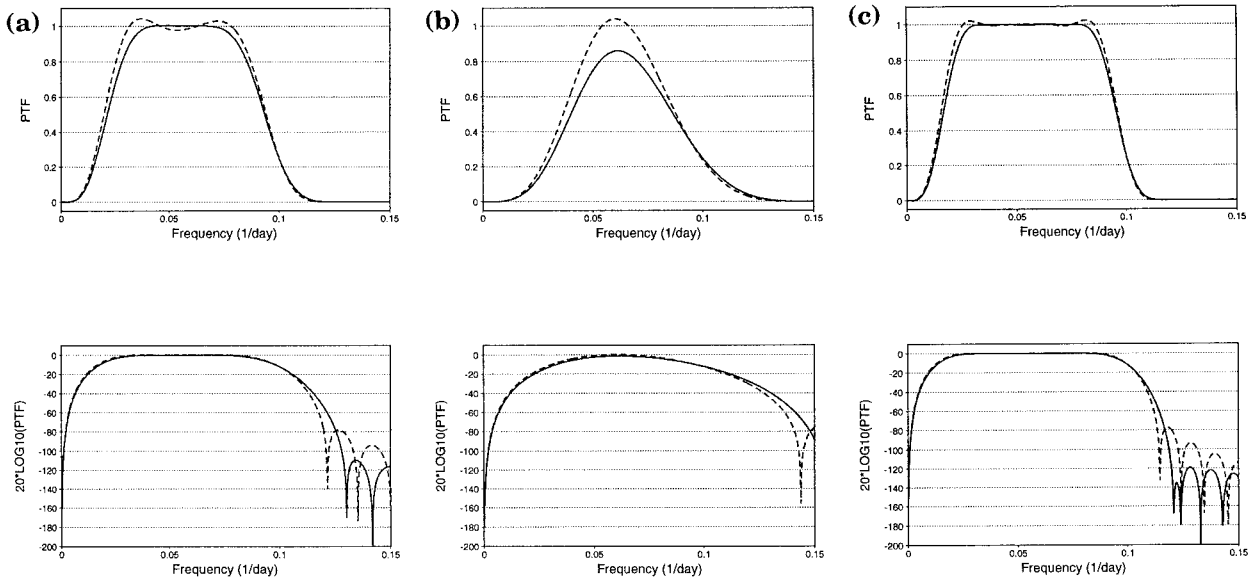

FIG. 1. (a) Power transfer function in linear (up) and logarithmic (down) scales for the Dolph (solid) and Bloomfield (dashed) versions of the bandpass filter with $S = 30$, $\theta_c^u = 2\pi/10$ and $\theta_c^l = 2\pi/90$. (b) and (c) Same as (a), but for $S = 15$ and 45, respectively.

10–90 time units bandpass filter. In Fig. 1a results for $S = 30$ are plotted. The upper panels show the power transfer function $T(\theta)$, whereas the response in *dB*, computed as

$$\alpha = 20 \log_{10} T(\theta), \tag{16}$$

is plotted in the lower panels. The Bloomfield filter (dashed line) shows nonmonotonic behavior in the two maxima at the edge of the pass band. The Dolph filter (solid line) does not have this problem; instead, the transition band is wider. In the logarithmic plot the ripples in the stop band are clearly seen and are higher for the Bloomfield version, although not by too much (a value of -80 dB corresponds to a variance attenuation out of the transition band of 1%, close to the ideal 0% attenuation). The wider transition band of the Dolph version can also be seen in the logarithmic plot, especially below -20 *dB* ($\theta = 0.11$ day^{-1}). The transfer function for filters with $S = 15$ and 45 are shown in Figs. 1b and 1c, respectively. For $S = 15$, the transition band is too wide. This problem is so bad for the Dolph version that even the pass band is smoothed by the convergence window, heavily reducing the performance of the filter. The increased sharpness obtained with the Bloomfield version allows it to be used when only a small span is possible. To prevent this problem, given a pass band width, an upper limit for the transition band width must be defined. A possible criterion is to avoid having the convergence window operating on the left-hand side of the pass band affect the right-hand side and vice versa. This can be expressed as $\delta + \theta_c^l < \theta_c^u - \delta$, or

$$\delta < \frac{\theta_c^u - \theta_c^l}{2}, \tag{17}$$

which gives the following lower limit for the filter span:

$$S > \frac{2T_c^u T_c^l}{T_c^u - T_c^l} - \frac{1}{2}, \tag{18}$$

where T_c^x is the cutoff period corresponding to θ_c^x. This relation holds approximately for any filter. A minimum span may be defined that in our example is $S_{\min} = 22$. The $S = 45$ filter gives slightly better performance for both versions, reducing the transition band as expected. A larger span produces better results in the transition band at the expense of losing a larger number of endpoints from the time series. It is noticeable from Fig. 1c that the ripples for $S = 45$ are smaller for the Dolph version than in the $S = 30$ case (see logarithmic plot). Instead, for the Bloomfield version the greatest ripple produces again an attenuation of -80 *dB*.

A simple flexible procedure for designing a bandpass filter has been proposed that incorporates the use of any chosen convergence window. Given the upper and lower cutoff frequencies, Eqs. (14) and (15) provide simple analytic expressions for the bandpass filter weights. The minimum filter span can be estimated using Eq. (18). This procedure for designing a bandpass filter can easily incorporate any desired convergence window.

3. Application to midlatitude variability

a. Low-frequency intraseasonal variance

Two types of IS variability may be identified in the midlatitude circulation: one associated with low-fre-

quency phenomena and the other produced by higher-frequency synoptic-scale disturbances. The first is associated with processes having periods longer than the deterministic predictability time of roughly 10 days (Ghil and Mo 1991), whereas the higher-frequency variability is mainly produced by baroclinic instabilities (Blackmon 1976). In this section, we present the variability ranging from about 10 days up to a season, or low-frequency IS variability, as an illustrative example of the bandpass filtering. Knowledge about low-frequency IS variability modes is increasingly important in extended-range forecasting and is often poorly simulated by models. A review of the different phenomena that contribute to the low-frequency IS spectral band may be found in Ghil and Mo (1991). We have isolated this latter variability over the Northern Hemisphere in the analyses and in GCM simulations by using the above-described filtering procedure.

Simulations from the Météo-France GCM ARPEGE have been used in this work. The model has been adapted from the spectral atmosphere operational forecasting model used in France for the simulation of the tropospheric and stratospheric climate. The basic climate version is described in Déqué et al. (1994) (version 0) and Déqué and Piedelievre (1995) (version 1). A new version (version 2) of the model has recently been developed, which includes some new parameterizations. In a broad sense the main differences between the previous versions and the present one are the number of vertical levels (41 in this case), a new radiation scheme (Morcrette 1991), a crude version of the orographic gravity wave drag scheme by Lott and Miller (1997), the introduction of a convective gravity wave drag parameterization (Bossuet et al. 1997), improvements in the soil-vegetation scheme (ISBA) for deep soil magnitudes (Mahfouf et al. 1995), and a new and more realistic snow scheme (Douville et al. 1995). Prescribed observed sea surface temperatures are used. They are calculated daily by linear interpolation of the monthly mean Center for Ocean–Land–Atmospere Studies Climate Analysis Center at NOAA (COLA CAC) analyses of observed sea surface temperatures. Model orography is obtained by interpolating the high-resolution U.S. Navy data onto the Gaussian model grid. Two 10-yr-long runs have been used. One has been made with the version 1 of the model (henceforth ARPEGE1) and the other with version 2 (henceforth ARPEGE2). Both used T42 triangular truncation. For the sake of comparison, daily Northern Hemisphere 500-hPa geopotential height European Centre for Medium-Range Weather Forecasts (ECMWF) reanalyses from 1980 to 1994 have been considered. This set comes from the global 31 level T106 analyses made in the framework of the ECMWF Reanalysis Project (henceforth ERA) (Gibson et al. 1996).

Digital bandpass filters have been applied to daily time series from which the time mean value has been removed. In the analysis of time series it is often desirable to remove strong periodicities, such as the annual cycle (Fuenzalida and Rosenbluth 1990), which are responsible for nonstationarity. This process, known as prewhitening, has also been applied by removing a daily mean annual cycle. The parameters chosen to estimate IS low-frequency variability are, as in the example, $\theta_c^u = 2\pi/10$, $\theta_c^l = 2\pi/90$, and $S = 30$. Subsequently, the mean standard deviation of the filtered time series for each season at each grid point is calculated. Only results for winter are presented here. In Fig. 2a, the standard deviation of the Dolph version applied to the ERA data is shown. Maxima are located mainly over the northern part of the oceans and western Siberia. Absolute maxima are found over the northeastern Pacific in winter and the northwestern Atlantic in spring (not shown). The smallest values are observed in summer (not shown). These features are not very sensitive to the period chosen as reference. Some additional computations show that results remain essentially the same when the period 1984–93 is considered.

A clear underestimation of the filtered variance is observed in the model results (Fig. 2b), in good agreement with Reynolds et al. (1996). A large eastward shift of the maxima is observed for ARPEGE1, especially over the North Atlantic, and is also present in spring (not shown). Figure 3 shows the square root of the difference in the filtered variance. The sign is set after finding the square root. Important model overestimation is present over southern Eurasia, as can be seen in Fig. 3a, associated with the southward phase shift in the regions of maximum variability. ARPEGE2 shows increased variability amounts compared with the older version, as observed in Fig. 2c, producing a reduced underestimation compared to ERA (Fig. 3b). The improvement is most marked in winter, and it has been also observed in blocking frequency (not shown). A more detailed analysis of the model intraseasonal variability can be found in Doblas-Reyes et al. (1998, manuscript submitted to *Tellus*).

An intercomparison of the two filtering methods reveals that results are geographically the same after the application of either of them. Nevertheless, in order to draw a distinction between the performance of both bandpass filter versions, the square root of the difference in the filtered variance with Bloomfield and Dolph versions is presented in Fig. 4. In winter, the Bloomfield version offers greater variance (around 20%), and the same thing is found for every dataset, every season, and any filter span. Similar results have been obtained with different pass band widths. This is normal as the area of the power transfer function of the Bloomfield version is slightly higher (see Fig. 1). However, the 20% value has no direct correspondence with the difference in integrated areas for each transfer function. In a very simplified scheme, the lower the frequency of the atmospheric fluctuations, the greater the amplitudes. Thus, a small difference in the transfer function in the low-frequency part of the spectrum can produce an important

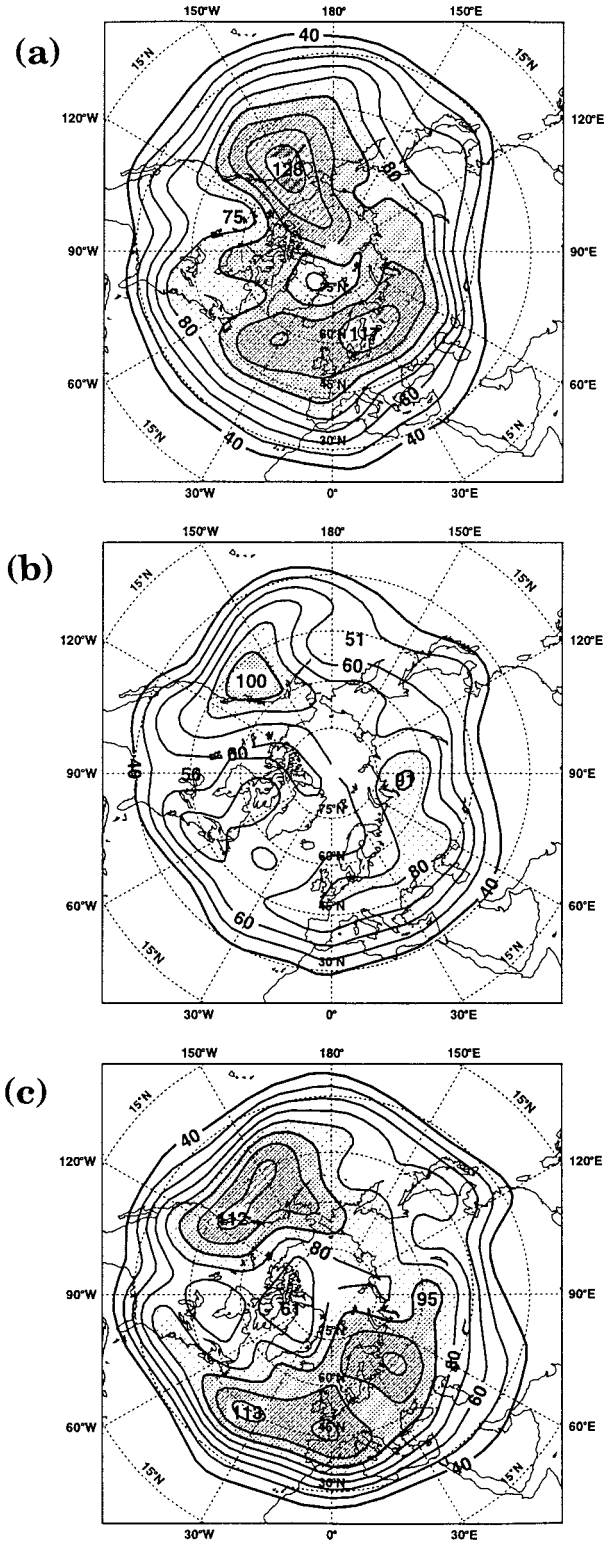

FIG. 2. (a) Winter standard deviation of 10–90-day bandpass filtered ERA data with the Dolph version and $S = 30$. Contour interval 10 m. Regions with values greater than 80 m are hatched. (b) and (c) Same as (a) but for ARPEGE1 and ARPEGE2 data, respectively.

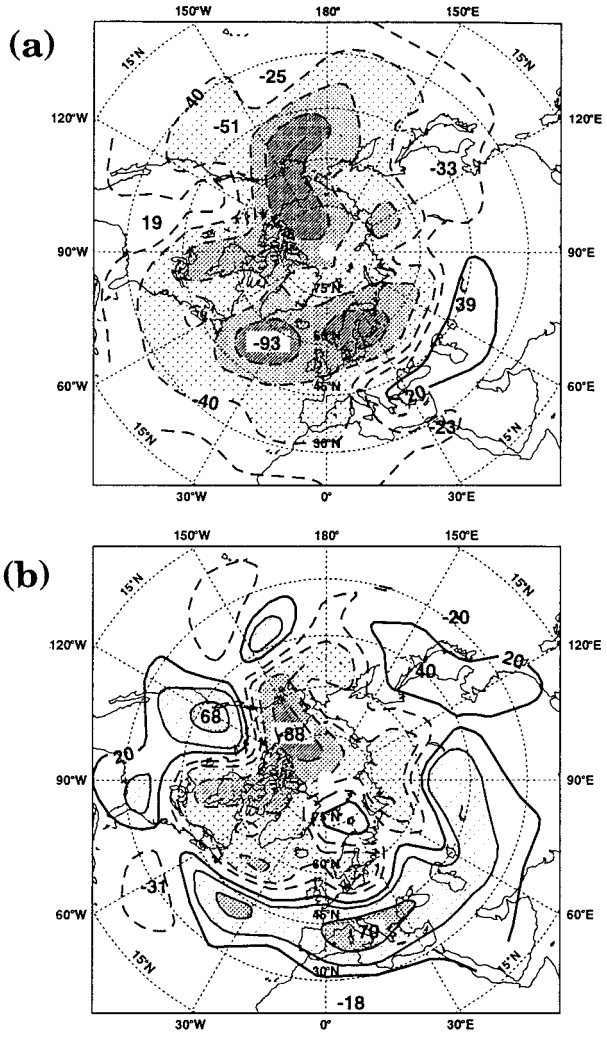

FIG. 3. (a) Square root of the differences in the 10–90-day bandpass filtered (Dolph version and $S = 30$) variance for winter between ARPEGE1 and ERA data. The sign is set after computing the square root. Contour interval 20 m. Regions with absolute values greater than 40 m are hatched. (b) Same as (a) but for ARPEGE2 and ERA data.

increase in the filtered variance. This increment has a similar spatial pattern to that of the filtered variance. This is due to the continuity of the atmospheric spectrum, which diminishes the beneficial role of the convergence windows. However, in other applications, if a strong signal is present in the spectrum and is found inside the pass band, the Gibbs oscillations could cause it to be underweighted.

A low-pass filter similar to the one computed by Blackmon (1976) has been constructed and also been applied to the datasets. This is a linear filter emphasizing periods greater than 10 days, retaining both IA and IS variability. Regions of low-frequency variability maxima remain essentially in the same location (not shown) for both ERA data and model results. This result cannot

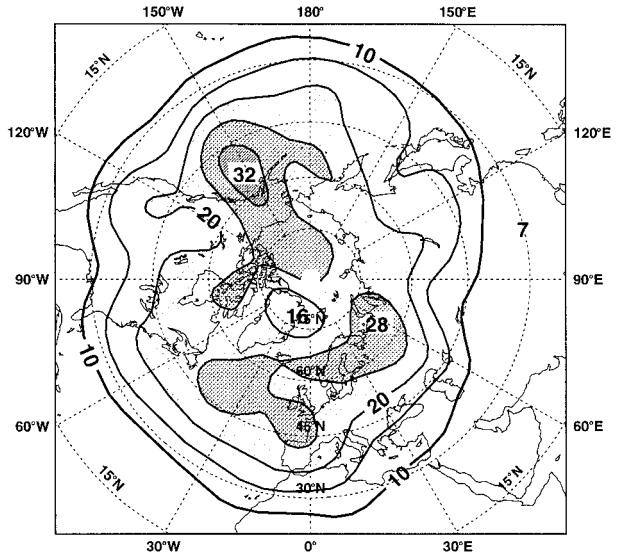

FIG. 4. Square root of the differences in the 10–90-day bandpass filtered variance between Bloomfield and Dolph versions ($S = 30$) in ERA data for winter. The sign is set after computing the square root. Contour interval 5 m. Regions with values greater than 20 m are hatched.

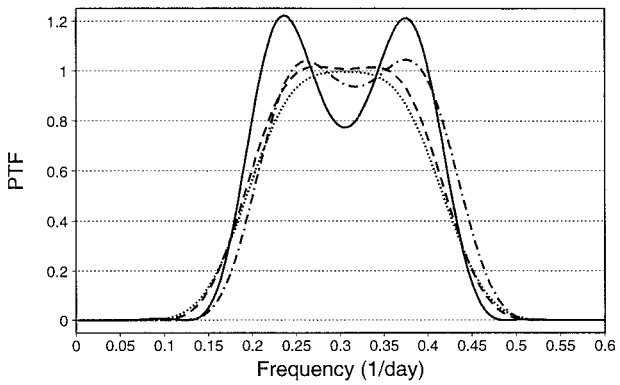

FIG. 5. Power transfer function for the least squares (solid), Dolph (dotted), and Bloomfield (dashed) versions of the 2.2–6-day bandpass filter with $S = 30$. The dot-dashed line corresponds to the transfer function of the Blackmon (1976) bandpass predefined filter.

be attained by just using the predefined Blackmon, which includes both IA and IS types of variability.

b. Structure of synoptic-scale baroclinic fluctuations

One-point correlation maps of the 2–6-day filtered geopotential height have been used for investigating the three-dimensional structure of the extratropical synoptic-scale fluctuations (e.g., Blackmon et al. 1984). This problem has been analyzed here as an example of the usefulness of the filtering method proposed in section 2. Three different filters have been used: the 2.2–6-day Blackmon bandpass medium-scale filter [weights have been taken from Blackmon (1976)] and the Bloomfield and Dolph versions of the bandpass filter. The last two have a similar pass band to the predefined (Blackmon) filter. The predefined filter uses $S = 15$ for twice-daily data. The others have $S = 30$ for 6-hourly data, all of them removing 6.5 days at the end of each time series. The frequency responses along with the response of the least squares bandpass filter are shown in Fig. 5. The least squares filter contains significant Gibbs oscillations, such that a fluctuation with a period of 5 days will be amplified 20% in variance and another with a period of 3 days will show a 20% decrease. The effect of the convergence windows is to smooth those oscillations, at the expense of widening the transition band. Gibbs phenomena are also present in the Blackmon power transfer function, although they are significantly smaller.

The data used for computing the one-point correlation maps are the 6-hourly ECMWF geopotential height analyses for the 1996–97 extended winter (November–April) at seven standard levels: 500, 300, 200, 150, 100, 70, and 50 hPa (0000 and 1200 UTC data have been used for the Blackmon filter). The horizontal structure of the fluctuations on the 300-hPa surface for the 45°N, 60°W base point at the 500-hPa surface from the three filtered versions is presented in Fig. 6. These fluctuations present an east–west-oriented zonally wavelike structure, with a zonal wavelength of about 4000 km. Their meridional structure is simple, with a maximum at the latitude of the base grid point and amplitude decreasing smoothly to zero about 20° of latitude on either side. The wave train shows an equatorward component at the eastern end, which is more evident at higher levels (not shown). There is a striking similarity between all of the filtered versions, proving that 1) the signal is strong enough to not be affected by the type of filter used, 2) the new filters are at least as good as the predefined filter, and 3) the use of twice daily data is enough for such analyses. The mean period of the fluctuations is about 4 days, as observed in the one-point correlation maps at lags -2 and $+2$ days (not shown). The evolving patterns are indicative of eastward propagating wave trains. The vertical structure has been presented in Lim and Wallace (1991), and similar results are found in this study (Fig. 7a). Correlation decreases from the base point and significant values are found up to the lower stratosphere, which can explain, as in Mote et al. (1991), the close relationship between total ozone and synoptic-scale baroclinic fluctuations. There exists a slight westward tilt of the waves with height, which decreases as one moves across the section from west to east. Successive maxima and minima appear at progressively higher levels as one moves eastward, indicating upward energy dispersion. The vertical structure does not show any dependence on the filter used. Similar conclusions can be inferred from other base points and reference levels, both over the Atlantic and the Pacific storm tracks.

It is important to determine to what extent these cor-

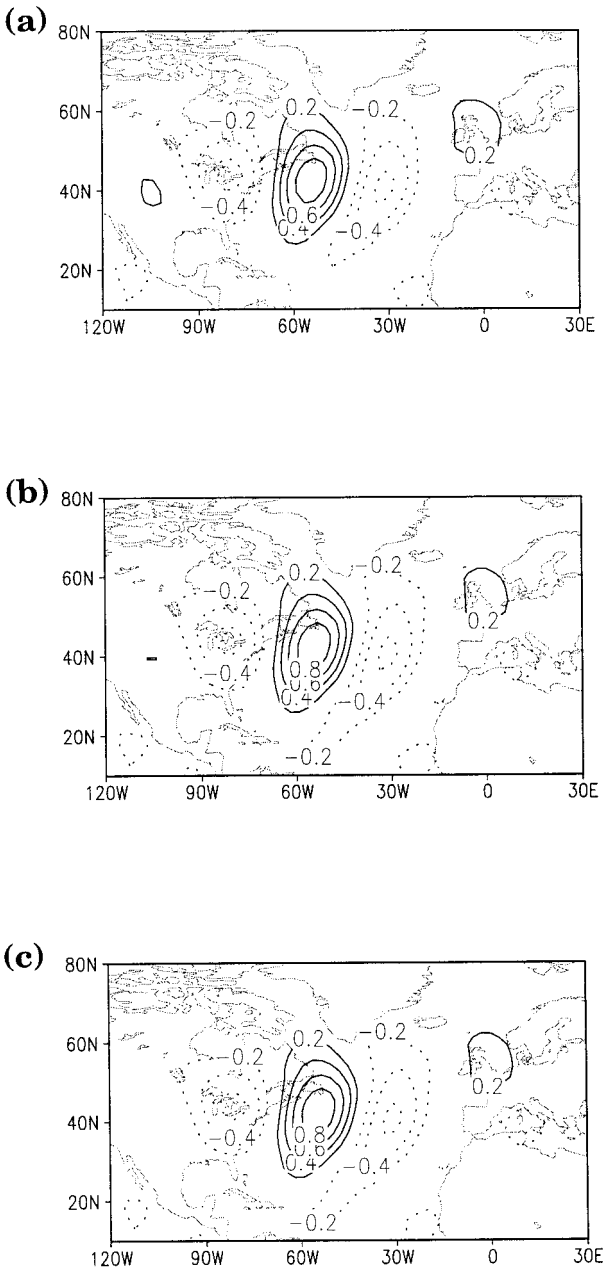

FIG. 6. Horizontal one-point correlation maps: 1996–97 extended winter correlation of 2.2–6-day bandpass filtered 300-hPa geopotential height with corresponding bandpass filtered 500-hPa geopotential height at the base point 45°N, 50°W. The filters used are a) Blackmon predefined bandpass filter, b) Bloomfield version, and c) Dolph version. Contour interval 0.2. The zero line is avoided.

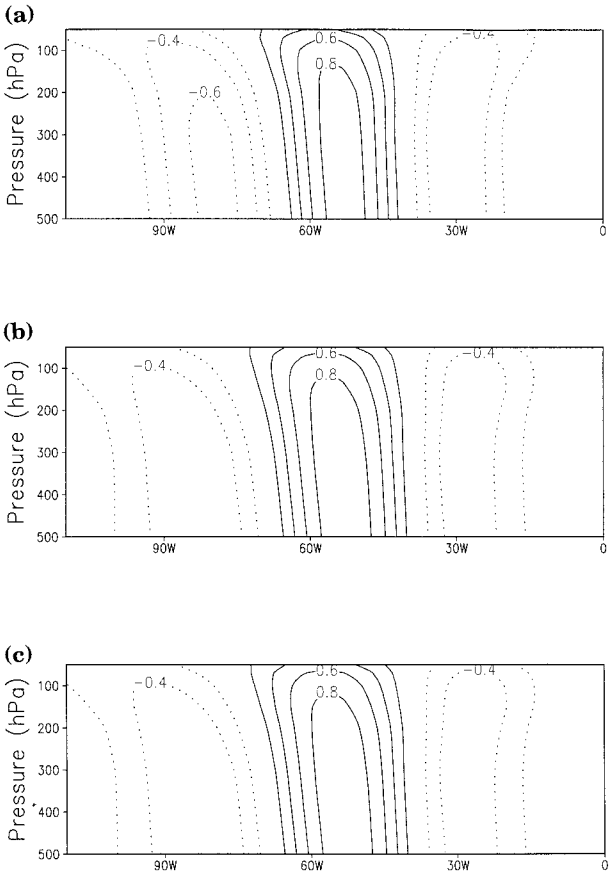

FIG. 7. Vertical one-point correlation maps: 1996–97 extended winter correlation of bandpass filtered geopotential height at seven levels with corresponding bandpass filtered 500-hPa geopotential height at the base point 45°N, 50°W. The filters used are a) 2.2–6 day Blackmon predefined bandpass filter, b) 2.2–10-day Bloomfield version, and c) 2.2–10-day Dolph version. Contour interval 0.2. The zero line is avoided.

relation patterns are influenced by the pass band width used. To this end a full set of bandpass filters has been generated by simply changing the lower cutoff frequency in the analytic filters (the Blackmon filter is predefined, so it is not possible to change it). The filter weights are easily obtained using the analytic expressions proposed above. Several pass band widths have been considered. In Fig. 7, the vertical structure at 45°N for the Blackmon filtered data and for the two 2.2–10-day analytic bandpass filtered versions with the former base point is shown. It can be observed that the wavelength of the correlation patterns increases when decreasing the lower cutoff frequency (i.e., when increasing the pass band width). The wavelength increase is around 10% for a 2.2–10-day bandpass filter and it is greater in the western part of the vertical section. Similar results are found with the two versions of the bandpass filter. A small decrease in correlation is also observed. The horizontal patterns (not shown) have larger meridional extents than observed with the narrower filters. They penetrate farther south into the subtropical region and farther north into the subpolar region. An important feature is that over the storm track areas the period of the fluctuations is slightly higher than 4 days, as the 2-day lagged one-point correlation maps (not shown) are not exactly in quadrature with the simultaneous correlation maps. With larger pass band, a clearer correlation

structure emerges in the end of the Atlantic storm track. A region of significant correlation over western Europe is observed in the evolving pattern, which is not present with the narrower bandpass filters, showing that over this area the more barotropic fluctuations can have a longer period.

Finally, Mote et al. (1991) suggest that the longer-scale baroclinic waves are better able to penetrate into the stratosphere, and therefore one might expect to see larger correlations in the stratosphere by increasing the pass band width. Interestingly, this does not appear to be the case, and this is discussed in more detail in Orsolini et al. (1998).

4. Summary

A simple analytic procedure for designing general digital bandpass filters has been presented. The bandpass filter is constructed from the difference of two low-pass filters and is defined by a set of three parameters: the filter span (S), and the lower and upper cutoff frequencies of the pass band. Convergence windows can easily be convolved with the bandpass filter in order to remove Gibbs oscillations and improve its performance. Two convergence windows have been considered here: the Bloomfield and the Dolph windows. Both versions give a good transfer function that mimics the ideal box function. The Bloomfield version has a steeper transition band than the Dolph version but is not monotonic at the edge of the pass band, producing some spurious oscillations in the transfer function. The Dolph version avoids this problem but requires a greater span to give a narrow pass band, which may be useful in some specific cases (Valero et al. 1996). Two main advantages of the method presented here over predefined filters are that an analytic expression for flexibly computing the filter weights is provided and that any preferred convergence window can be easily applied.

In order to illustrate the method, two examples have been considered. The 10–90-day low-frequency IS filtered variance in midlatitudes from both ECMWF reanalyses and simulations by the GCM ARPEGE has been computed. The model underestimates low-frequency IS variance in the same way as the whole low-frequency variance. Geographical differences between Bloomfield and Dolph filtered versions are not very important because of the continuity of the atmospheric spectrum, though the first version retains slightly more variance than the Dolph version. The sensitivity to the filter span is also quite small. The structure of the synoptic-scale baroclinic fluctuations during the 1996–97 extended winter has also been studied. It is shown that the horizontal and vertical structure of these fluctuations does not depend very much on the frequency band up to a period of 10 days, showing an increase in wavelength as lower-frequency fluctuations are considered. Their vertical propagation is not sensibly affected by lower-frequency fluctuations.

Results show that the method presented in this paper has an advantage over predefined filters in that it allows one to easily estimate the atmospheric fluctuations in arbitrarily chosen frequency bands of interest.

Acknowledgments. This study would not have been possible without the kind help provided by A. Braun and the scientists at Météo-France and ECMWF who develop and run the ARPEGE-IFS model. Special thanks go to Dr. David B. Stephenson for both useful advice and discussions and for reviewing the manuscript. M. J. Casado and A. Pastor (INM) made a great effort in reviewing both routines and draft versions of the text. P. Lynch and J.-P. Ceron also carefully read the manuscript and offered some interesting ideas. Finally, we gratefully appreciate the helpful reviewers' comments, which had a substantial impact on this paper. This work has been partly supported by the Consejería de Educación de la Comunidad de Madrid (Spain) and by the European Commission (Contract ENV4-CT95-0184).

REFERENCES

Blackmon, M. L., 1976: A climatological spectral study of the 500-mb geopotential height of the Northern Hemisphere wintertime circulation. *J. Atmos. Sci.,* **33,** 1607–1623.

——, and N.-C. Lau, 1980: Regional characteristics of the Northern Hemisphere wintertime circulation: A comparison of the simulation of a GFDL general circulation model with observations. *J. Atmos. Sci.,* **37,** 497–514.

——, Y.-H. Lee, and J. M. Wallace, 1984: Horizontal structure of 500-mb height fluctuations with long, intermediate, and short timescales. *J. Atmos. Sci.,* **41,** 961–979.

Bloomfield, P., 1976: *Fourier Analysis of Time Series: An Introduction.* Wiley, 258 pp.

Bossuet, C., M. Déqué, and D. Cariolle, 1997: Impact of a simple parameterization of convective gravity wave drag in a stratosphere–troposphere general circulation model and its sensitivity to vertical resolution. *Ann. Geophys.,* **16,** 238–249.

Christoph, M., U. Ulbrich, and U. Haak, 1995: Faster determination of the intraseasonal variability of storm tracks using Murakami's recursive filter. *Mon. Wea. Rev.,* **123,** 578–581.

Déqué, M., and J. P. Piedelievre, 1995: High resolution climate simulation over Europe. *Climate Dyn.,* **11,** 321–339.

——, C. Dreveton, A. Braun, and D. Cariolle, 1994: The ARPEGE/IFS atmospheric model: A contribution to the French community climate modelling. *Climate Dyn.,* **10,** 249–266.

Doblas-Reyes, F. J., M. Déqué, D. B. Stephenson, and F. Valero, 1998: North-Atlantic wintertime intraseasonal variability and its sensitivity to GCM horizontal. *Tellus,* in press.

Dolph, C. L., 1946: A current distribution for broadside arrays which optimizes the relationship between beam width and side-lobe level. *Proc. IRE,* **34,** 335–348.

Douville, H., J. F. Royer, and J.-F. Mahfouf, 1995: A new snow parameterization for the Météo-France climate model. Part II: Validation in a 3D GCM experiment. *Climate Dyn.,* **12,** 37–52.

Duchon, C., 1979: Lanczos filtering in one and two dimensions. *J. Appl. Meteor.,* **18,** 1016–1022.

Enting, I. G., 1987: The interannual variation in the seasonal cycle of carbon dioxide concentration at Mauna Loa. *J. Geophys. Res.,* **92,** 5497–5504.

Fuenzalida, H., and B. Rosenbluth, 1990: Prewhitening of climatological time series. *J. Climate,* **3,** 382–393.

Ghil, M., and K. Mo, 1991: Intraseasonal oscillations in the global

atmosphere. Part I: Northern Hemisphere and Tropics. *J. Atmos. Sci.,* **48,** 752–779.

Gibson, R., P. Kallberg, and S. Uppsala, 1996: The ECMWF reanalysis (ERA) project. *ECMWF Newsl.,* **73,** 7–16.

Hamming, R. W., 1977: *Digital Filters.* Prentice-Hall, 226 pp.

Hoskins, B. J., H. H. Hsu, I. N. James, M. Masutani, P. D. Sardeshmukh, and G. H. White, 1989: Diagnostics of the global atmosphere circulation based on ECMWF analyses 1979–1989. WMO/TD 326, 217 pp.

Huang, X.-Y., and P. Lynch, 1993: Diabatic digital filtering initialization: Application to the HIRLAM model. *Mon. Wea. Rev.*, **121,** 589–603.

Kousky, V. E., and M. T. Kayano, 1994: Principal modes of outgoing longwave radiation and 250-mb circulation for the South American sector. *J. Climate,* **7,** 1131–1143.

Lanzante, J. R., 1996: Lag relationships involving tropical sea surface temperatures. *J. Climate,* **9,** 2568–2578.

Lim, G. H., and J. M. Wallace, 1991: Structure and evolution of baroclinic waves as inferred from regression analysis. *J. Atmos. Sci.,* **48,** 1718–1732.

Lott, F., and M. Miller, 1997: A new sub-grid scale orographic drag parametrization: Its formulation and testing. *Quart. J. Roy. Meteor. Soc.,* **123,** 101–128.

Lynch, P., 1997: The Dolph–Chebyshev window: A simple optimal filter. *Mon. Wea. Rev.,* **125,** 655–660.

——, D. Giard, and V. Ivanovici, 1997: Improving the efficiency of a digital filtering scheme for diabatic initialization. *Mon. Wea. Rev.,* **125,** 1976–1982.

Mahfouf, J.-F., A. O. Manzi, J. Noilhan, H. Giordani, and M. Déqué, 1995: The land surface scheme ISBA within the METEO-FRANCE climate model ARPEGE. Part I: Implementation and preliminary results. *J. Climate,* **8,** 2039–2057.

Morcrette, J. J., 1991: Radiation and cloud radiative properties in the European Centre for Medium Range Weather Forecasts forecasting system. *J. Geophys. Res.,* **96,** 9121–9132.

Mote, P. W., J. R. Holton, and J. M. Wallace, 1991: Variability in total ozone associated with baroclinic waves. *J. Atmos. Sci.,* **48,** 1900–1903.

Orsolini, Y. J., D. B. Stephenson, and F. J. Doblas-Reyes, 1998: Storm track signature in total ozone during the Northern Hemisphere winter. *Geophys. Res. Lett.,* **25,** 2413–2416.

Reynolds, C., R. Gelaro, and T. Murphree, 1996: Observed and simulated Northern Hemisphere instraseasonal circulation anomalies and the influence of model bias. *Mon. Wea. Rev.,* **124,** 1100–1118.

Valero, F., F. J. Doblas-Reyes, and J. F. González, 1996: On the long term evolution of seasonal precipitation in southwestern Europe. *Ann. Geophys.,* **14,** 976–985.